

pubs.acs.org/ac Article

# A Nanojunction pH Sensor within a Nanowire

Nicholas P. Drago, Eric J. Choi, Jihoon Shin, Dong-Hwan Kim, and Reginald M. Penner\*



Cite This: Anal. Chem. 2022, 94, 12167–12175



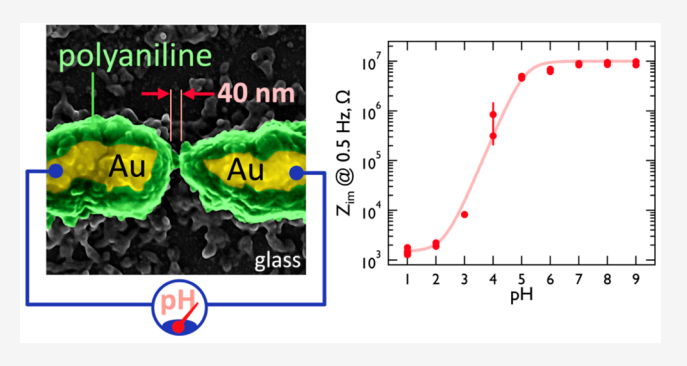
**ACCESS** I

Metrics & More

Article Recommendations

Supporting Information

ABSTRACT: pH sensors that are nanoscopic in all three dimensions are fabricated within a single gold nanowire. Fabrication involves the formation of a nanogap within the nanowire via electromigration, followed by electropolymerization of pH-responsive poly(aniline) (PANI) that fills the nanogap forming the nanojunction. All fabrication steps are performed using wet chemical methods that do not require a clean room. The measured electrical impedance of the PANI nanojunction is correlated with pH from 2.0 to 9.0 with a response time of 30 s. Larger, micrometer-scale PANI junctions exhibit a slower response. The measured pH is weakly influenced by the salt concentration of the contacting aqueous solution. An impedance



measurement at two frequencies (300 kHz and 1.0 Hz) enables estimation of the salt concentration and correction of the measured pH value, preserving the accuracy of the pH measurement across the entire calibration curve for salt concentrations up to 1.0 M. The result is a nanoscopic pH sensor with pH sensing performance approaching that of a conventional, macroscopic pH glass-membrane electrode.

The measurement of pH is fundamental to understanding and controlling a diverse range of chemical and biological phenomena occurring in aqueous solutions. The glass membrane pH electrode, dating back to the early 1900s, permits the pH of a solution to be correlated with a transmembrane dc potential that is measurable in seconds under optimal conditions. Miniaturization of the glass pH electrode to the  $60-80~\mu m$  scale for measurements of single cells was demonstrated in 1964 using glass micropipettes. These micropipette pH sensors are macroscopic in length but microscopic in diameter with modern versions in the  $1-5~\mu m$  diameter range. Nanometer-scale pH probes capable of still higher spatial resolution require other architectures and transduction mechanisms.

Lieber and co-workers<sup>4</sup> fabricated the first single nanowire-based pH sensor in 2001. These authors employed electron-beam lithography to fabricate a 10–20 nm  $\times$  2–4  $\mu$ m silicon nanowire field effect transistor (SiNW FET) that was functionalized with 3-aminopropyltriethoxysilane (APTES). This sensor transduced pH using dc conductance. This is still the only prior example of a single nanowire-based pH sensor, as far as we are aware.

Several optical pH sensors with nanometer-scale dimensions have been described (Table S1). Fujisaku et al.<sup>5</sup> used chemically modified diamond nanocrystals containing nitrogen vacancies to optically transduce pH. In their study, the relaxation of electron spins of the nitrogen vacancies was correlated with the local pH environment.<sup>5</sup> Shen et al.<sup>6</sup> demonstrated pH sensing using gold nanoclusters modified

with L-/D-cysteine by measuring the phosphorescence after the self-assembly of microstructures from the gold nanoclusters.<sup>6</sup>

Electronically conductive polymer nanojunction sensors were pioneered by Nongjian Tao and co-workers. Table 11 Using an array of focused ion beam (FIB)-patterned metal gaps as electrical contacts, electropolymerization was used to form nanojunctions of poly(ethylenedioxythiophene) (PEDOT), poly(aniline) (PANI), and other conductive polymers, doped with chemically responsive molecules. Vapor sensors for detecting trinitrotoluene (TNT) were demonstrated. Solution phase sensors for detecting glucose, and redox active analytes such as dopamine and hydroquinone were also described.

PANI can also function as a resistance-based pH transducer. In its protonated, emeraldine salt state, PANI has high electrical conductivity (>10<sup>2</sup> S/cm). <sup>12</sup> Deprotonation of the salt to form the emeraldine base reduces the conductivity to 10<sup>-8</sup> S/cm, a difference of 10 orders of magnitude (Scheme S1). <sup>12</sup> Kaner and co-workers <sup>13,14</sup> employed PANI nanofibers for chemical sensing. This work demonstrated that nanostructured PANI could produce larger and more rapid resistance responses when exposed to acidic or basic vapors

Received: June 17, 2022 Accepted: August 12, 2022 Published: August 24, 2022





including as ammonia and HCl, compared to PANI films. In these experiments, the sensing element consisted of a mat of PANI nanofibers rather than single nanofibers. <sup>13,14</sup> Subsequently, Choi and co-workers <sup>15</sup> electropolymerized PANI with the same nanofiber mat morphology in lithographically fabricated 5  $\mu$ m  $\times$  3 mm microgaps for solution phase pH measurements.

To our knowledge no attempt has been made to create a single polymer nanojunction sensor for any analyte. In fact, few examples exist of single polymer nanowire sensors for any analyte in the literature. These have been achieved by drop-casting a nanowire slurry between many gold microelectrodes and using ac dielectrophoretic alignment to bridge the electrodes. Extra nanowires, beyond the one required, are then physically removed using a microprobe. 16,17 Scanned tip electrospinning has also been employed to create single PANI nanofibers between two gold electrodes, 18 but such nanofibers have not been applied to measurements in liquids. A third approach has involved chemical polymerization of aniline within trenches on surfaces formed by electron beam lithography. 19 The dc resistance of single PANI nanowires formed using this process was measured as it was exposed to solutions with different pH values. However, pH values above 4.5 were not accessible because of the excessive magnitude of the resistance in these experiments.<sup>19</sup>

Here, we demonstrate that PANI nanojunctions embedded within single gold nanowires can be reproducibly fabricated. These single nanojunctions (henceforth, NJ-pH sensors) transduce pH and generate an impedance signal that is measurable at the two nanowire contacts, producing a pH sensing "node" that is nanoscopic in all three dimensions. Moreover, we find that impedance allows for electrical signals to be measured far past the metal—insulator transition of PANI, at its p $K_{\rm a}\approx 4.0.$  NJ-pH sensors constitute a rapid-responding (30 s), reversible, reusable, and robust pH measuring system with a wide pH dynamic range of 2.0–9.0.

## **■ EXPERIMENTAL SECTION**

**Materials.** All chemicals were used as purchased without further purification. Nickel pellets (99.995%) and Au pellets (99.999%) were purchase from the Kurt J. Lesker Company. Clean Earth Cyanide Free Plating Solution 24ct Yellow was purchased from Stuller.com. Aniline ACS reagent grade  $(\geq 99.5\%)$  and Phosphate-buffered saline (10x concentrate, BioPerformance Certified) were purchased from Sigma-Aldrich. Sodium phosphate (monobasic, anhydrous, enzyme grade >99%), sodium phosphate dibasic (heptahydrate, 99.4%), sodium chloride (≥99.0%), nitric acid (certified ACS Plus), concentrated sulfuric acid (certified ACS Plus), Ricca chemical synthetic urine solution, and concentrated hydrochloric acid (certified ACS Plus) were purchased from Fisher Scientific. Lithium perchlorate (>99%) was purchased from Arcos Organics. Microposit S1808 positive photoresist and Microposit MF-319 developer were purchased from Kayaku Advanced Materials.

**Single Au Nanowire Fabrication.** The electrodeposition of single gold nanowires was accomplished using the lithographically patterned nanowire electrodeposition (LPNE) process, as previously described (Figure S1 steps 1–5).<sup>20</sup>

**Electromigration.** The automated, feedback-controlled electromigration process used to prepare nanogaps in single

gold nanowires has been described elsewhere and is shown step 10 (Figure S1).<sup>21</sup>

Poly(aniline) Electropolymerization. The electropolymerization of PANI onto the gold nanowire containing a nanogap was performed in aqueous 0.1 M aniline, 0.5 M H<sub>2</sub>SO<sub>4</sub> using a three-electrode cell in which the fractured nanowire, contacted on both ends, served as the working electrode in conjunction with a mercurous sulfate reference electrode (MSE) and a platinum counter electrode (Figure S1, step 11). Cyclic voltammetry was used to initiate the electropolymerization PANI using five consecutive scans from -0.1 V to +0.6 V vs MSE at 50 mV/s. Continued growth of the PANI layer was then carried out for 10-20 growth cycles by sweeping from -0.1 to +0.45 V vs MSE at 50 mV/s until the nanogap was filled with PANI, as indicated by a stepwise reduction in the low frequency wire impedance, measure in situ. This two-step process involving decreasing the positive potential limit after the nucleation scans enabled the electropolymerization of a highly uniform PANI layer while avoiding overoxidation of the polymer. 22 A PalmSens3 potentiostat running v2.8 software was used to perform electropolymerization.

PBS Buffers for pH Sensing. PBS pH buffers were prepared starting with a solution of 1× PBS. This PBS was titrated with 1.0 M HCl until the buffer was pH 1.0. An aliquot of the pH 1.0 buffer was taken, and the rest of the solution was back-titrated with 1.0 M NaOH until each desired pH was reached, with removal of an aliquot at each pH.

Electrochemical Impedance Spectroscopy. Electrochemical impedance spectroscopy (EIS) was performed using a Palmsens3 potentiostat running v2.8 software, a Princeton Applied Research 2263 potentiostat, or a Biologic potentiostat running EC-lab software. Measurements were acquired using a 10 mV ac amplitude at the rest potential of the nanowire. For temporally resolved pH measurements, a frequency of 5 Hz was used, and the impedance was sampled at 2 s intervals.

**Salt Correction.** Solutions with specified pH values and varying NaCl concentrations were prepared with a fixed, total phosphate concentration of 50 mM. This corresponded to the lowest salt concentration investigated in this study. Solutions with higher salt concentrations were obtained by adding NaCl to this phosphate buffer. pH was confirmed using a standard pH electrode measurement.

**Scanning Electron Microscopy.** Scanning electron microscopy (SEM) images were acquired using a FEI Magellan 400L XHR FE-SEM operating at an accelerating voltage of 10 keV. All samples were coated with 5 nm of iridium.

## ■ RESULTS AND DISCUSSION

Fabrication of Nanowire Nanojunction pH Sensors. We fabricated NJ-pH sensors in four steps (Figure 1). First a gold nanowire is prepared using lithographically patterned nanowire electrodeposition (LPNE, Figure S1). Second, gold contacts are applied (Figure 1a) and insulated by a photoresist overlayer (Figure 1b). A nanogap is then formed in the gold nanowire using feedback-controlled electromigration (Figure 1c). Finally, a nanojunction is formed by filling this nanogap with PANI by electropolymerization (Figure 1d). Although PANI coats the entire gold nanowire while forming the nanojunction, control experiments demonstrate that just the polymer within the nanojunction participates in pH transduction because only at the nanojunction is the throughwire impedance modulated by pH (Figures S2 and S3).

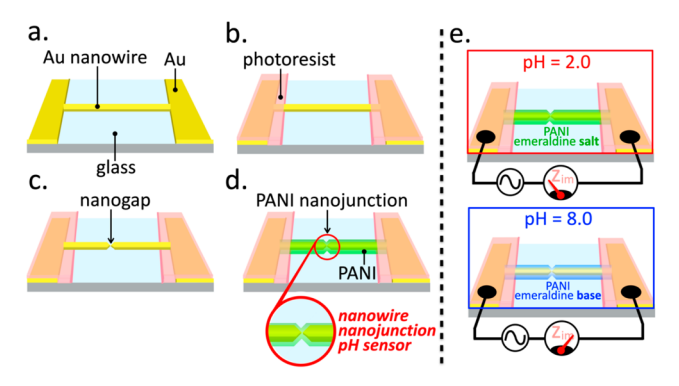


Figure 1. Fabrication of a NJ-pH sensor. (a) A gold nanowire (dimensions of 50  $\mu$ m (l), 100–200 nm (w), and 40 nm (h)) is prepared on a glass surface using lithographically patterned nanowire electrodeposition (LPNE). Gold electrical contacts to the nanowire are deposited by evaporation. (b) A photoresist layer insulates the gold contacts. (c) Feedback-controlled electromigration is used to produce a single nanogap (50  $\pm$  30 nm) within the nanowire, (d) Filling the nanogap with PANI using electropolymerization produces an NJ-pH sensor. (e) The imaginary component of the electrical impedance,  $Z_{\rm im}$ , is correlated with pH across the range 2.0–9.0 with a response time of 30 s.

The formation of the nanogap in step 3 is accomplished using feedback-controlled electromigration (Figure 2a). 21,24-30 This involves increasing the voltage applied to a gold nanowire,  $E_{\text{app}}$ , from an initial value of 10 mV at 5 mV/s while measuring the resistance of the nanowire. A reference resistance,  $R_{ref}$  is measured at the beginning of the experiment, and when the resistance of the nanowire changes by  $\pm 1.5\%$  of  $R_{\text{ref}}$  the  $E_{\text{app}}$  is decreased by 50 mV and a new  $R_{\text{ref}}$  is measured. 50 mV  $\hat{E}_{\text{app}}$ reductions are seen as glitches in the blue (resistance) and red  $(E_{app})$  traces (Figure 2a). The nanowire resistance decreases as the electromigration process proceeds because grain growth occurs in parallel with the formation of constrictions by electromigration and acts in opposition to the increase in resistance caused by these constrictions. A sudden increase in resistance at 600 s in Figure 2a signals the formation of a nanogap, terminating the electromigration program.

The anodic electropolymerization of aniline to form PANI on the nanowire and in the nanogap was accomplished using cyclic voltammetry (Figure 2b). From an initial potential of -0.10 V vs MSE, the potential was initially scanned at a rate of 50 mV/s to +0.60 V on five consecutive cycles to form PANI nuclei on all nanowire surfaces (Figure 2b). Then, an additional 20 growth scans to a positive limit of +0.45 V were performed to grow a conformal PANI layer over the entire nanowire, bridging the nanogap (Figure 2b). The

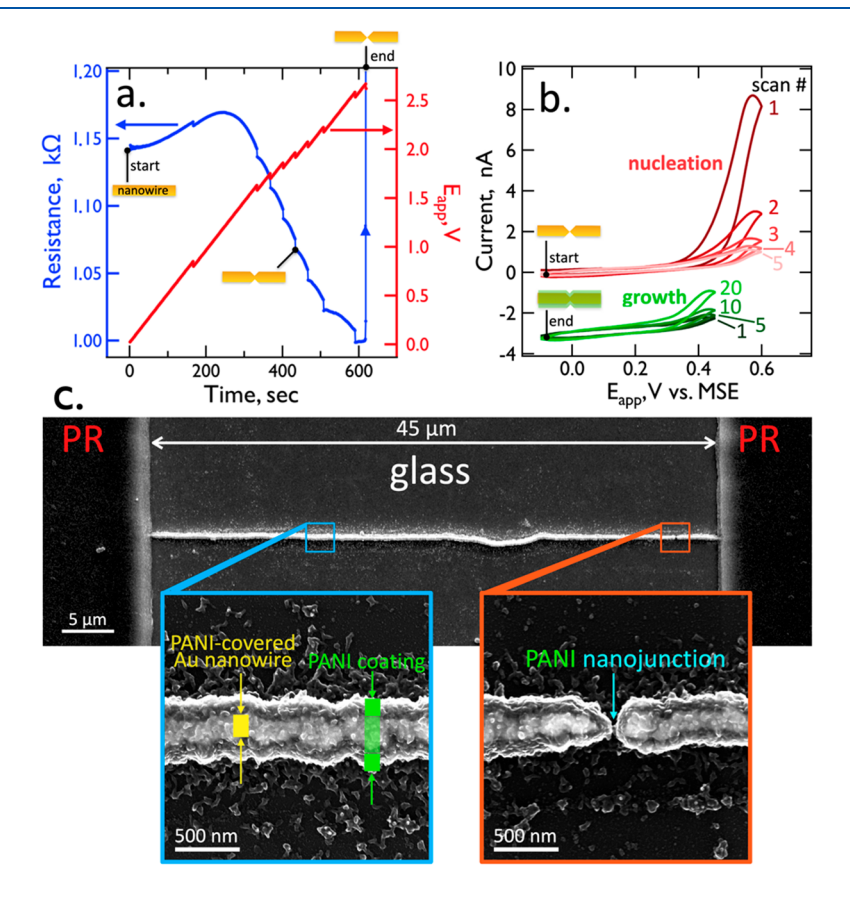


Figure 2. Fabricating a NJ-pH sensor. (a) Plot of the resistance of a gold nanowire (blue) and the applied potential (red) as a function of time during feedback-controlled electromigration to form a nanogap. Breaks in both curves indicate points at which the applied voltage was reduced by 50 mV. (b) Cyclic voltammograms (50 mV/s) for a bare gold nanowire with a nanogap in an aqueous 0.50 M  $H_2SO_4$  solution containing 0.1 M aniline. Five initial nucleation scans to a +0.60 V vs MSE positive limit prepare PANI nuclei on gold surfaces. A second series of 10-20 scans to +0.45 V grow a continuous PANI layer. These growth scans are terminated when electrical continuity across the nanojunction is detected. (c) SEM images of a PANI-coated Au nanowire containing a nanogap, showing at higher magnification (bottom) the PANI-coated gold nanowire and the PANI nanojunction.

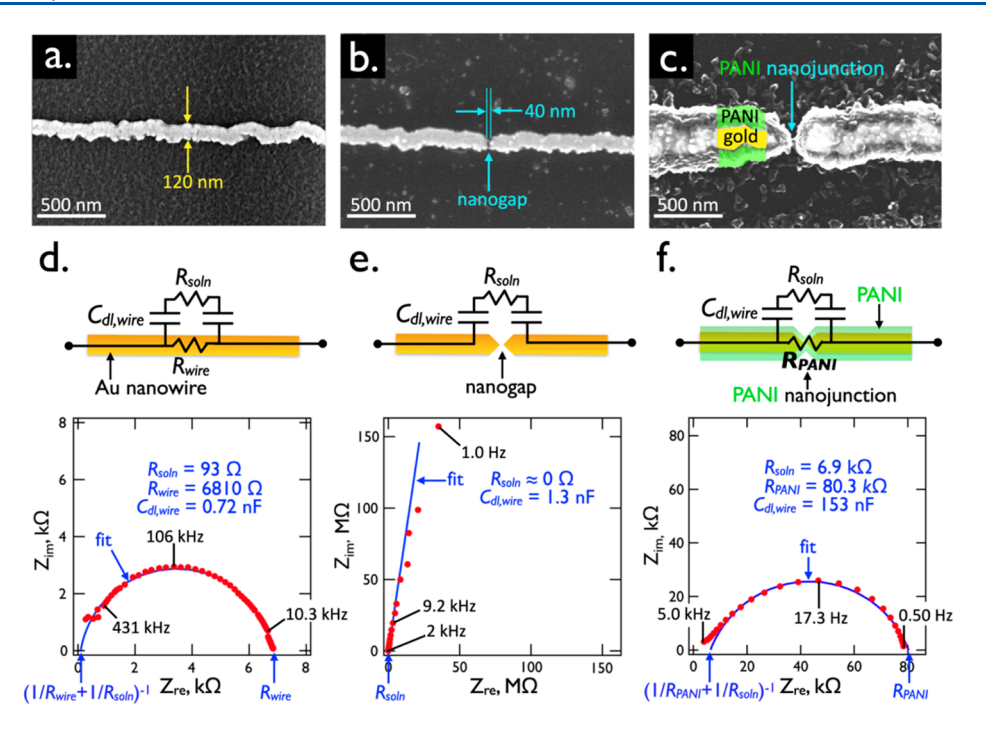


Figure 3. Impedance signatures for three types of nanowires. (a-c) SEM images of three types nanowires, as follows: (a) solid gold nanowire with dimensions 120 nm (w) and 40 nm (h), (b) solid gold nanowire containing a nanogap, and (c) solid gold nanowire containing a PANI nanojunction. (d-f). Equivalent circuit corresponding to each of these three nanowires (top), together with their characteristic Nyquist plots acquired in aqueous pH = 3.0 ( $Z_{im}$  versus  $Z_{re}$  as a function of frequency, as indicated, at bottom). In (d) and (f), semicircular Nyquist plots are produced by parallel resistors and capacitors, but impedance values are shifted by a factor of 10 in these two data sets. In (e), the nanogap eliminates the through-wire resistor and transforms the Nyquist plot into a near-vertical trace, approximating a series RC circuit. All Nyquist plots were acquired in aqueous pH = 3.0 phosphate buffer.

decrease in potential positive limit during the growth scans was used to prevent overoxidation of the polymer and to ensure a slow and controlled growth process. The slow PANI growth was monitored electrochemically and terminated when the through-wire resistance of the nanowire and nanogap was reduced to the  $k\Omega$  range, indicating PANI had formed a nanojunction by filling the gap and closing the circuit.

This fabrication process does not afford the ability to produce identical sensors with identical performance. While the reproducibility of the LPNE fabrication process for preparing the gold nanowire is excellent, the precision of the wire thickness and width dimensions is still subject to a variability of  $\approx\!10\%$  and  $20\!-\!30\%$ , respectively. The variability of the length of the nanogap formed by electromigration is >50%, leading to different required thicknesses of PANI forming the nanojunction and thus slightly different impedimetric properties between samples. Like the familiar glass electrode pH meter, each NJ-pH sensor requires calibration prior to use.

Scanning electron microscopy (SEM) images of PANI-coated gold nanowires (Figure 2c) demonstrate that the brighter gold nanowire core can be clearly distinguished from the PANI coating. A high degree of uniformity for the PANI coating is apparent from such SEM images. However, it should be appreciated that the dehydration of the PANI during evacuation of the SEM prior to imaging likely causes shrinkage of the PANI layer, and a reduction in its thickness as the polymer is dehydrated. Additionally, PANI nanoparticles can be seen around the nanowire because of the precipitation of the polymer near the nanowire during electropolymerization. We do not believe these particles influence the measurement

since the gold nanowire is much more conductive than PANI; thus only the PANI in the region where the gold nanowire is discontinuous will modulate the impedance.

**Signal Transduction.** Measurement of the electrical impedance has not been exploited to transduce nanowire sensors for any purpose, to our knowledge. In this application, impedance-based transduction enables higher signal-to-noise and confers the ability to correct the measured pH for the influence of salt in the test solution, as described below. To understand the impedance response of the NJ-pH sensor, it is instructive to compare the three device architectures shown in Figure 3: a solid gold nanowire (Figure 3a), a gold nanowire containing a nanogap (Figure 3b), and the nanowire nanojunction corresponding to a gold nanowire containing a nanogap coated with PANI (Figure 3c).

Shown in Figure 3 are experimental Nyquist plots of the impedance response for each circuit (red data), and the best fit corresponding to the equivalent circuit is shown in Figure 3d–f (blue data). The equivalent circuits for these three devices (Figure 3d–f) are constructed using just four circuit elements: the solution resistance ( $R_{\rm soln}$ ), the through-wire resistance of the gold nanowire ( $R_{\rm wire}$ ), a capacitor that accounts for the double-layer capacitance of the nanowire-solution interface ( $C_{\rm dl-wire}$ ), and in the case of the NJ-pH only, a resistor representing the PANI nanojunction ( $R_{\rm PANI}$ ).

Nyquist plots ( $Z_{\rm im}$  versus  $Z_{\rm re}$ ) as a function of frequency, f, show two limiting behaviors for these three devices: a semicircular plot, when C and R elements are electrically connected in parallel (Figure 3d,f), and a near-vertical plot, for a series RC circuit (Figure 3e). The values of the three circuit elements can be extracted by simulation, and these are

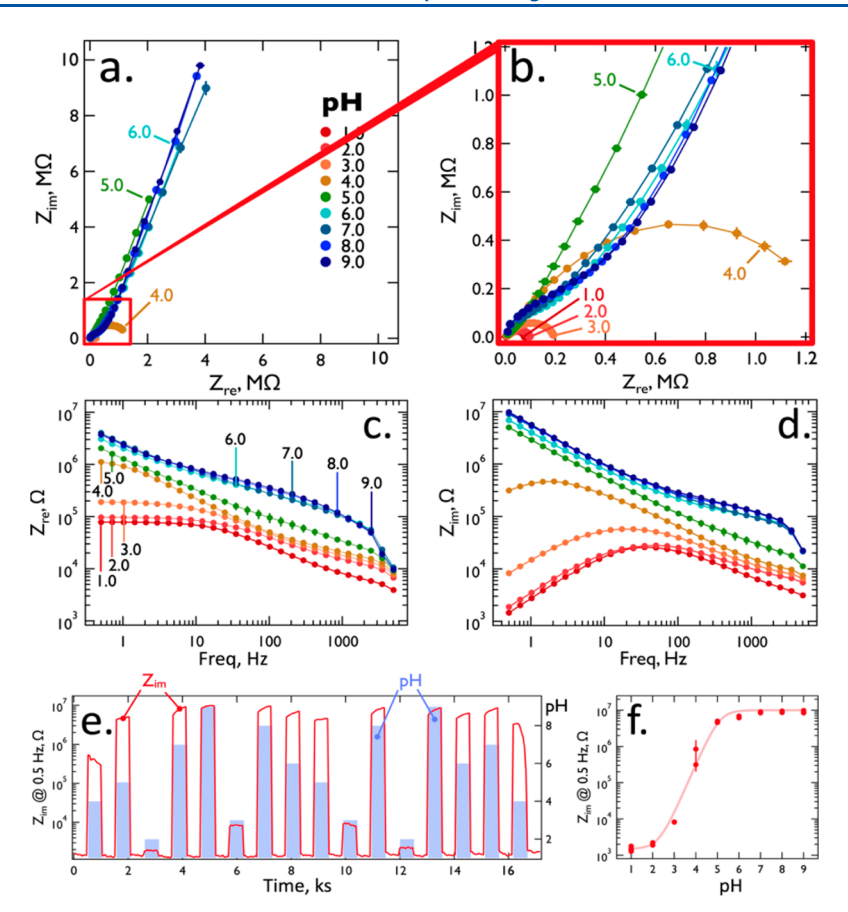


Figure 4. Randomized pH sensing with an NJ-pH sensor. (a, b) Nyquist plots for pH values of 1.0-9.0. At pH  $\leq 4.0$ , a semicircular trace is observed, consistent with the circuit shown in Figure 3f. At pH  $\geq 5.0$ , a near-vertical Nyquist plot is observed, as seen for Figure 3e, because the PANI has very low electronic conductivity in this pH range. (c, d) Plots of  $\log[Z_{\rm in}]$  and  $\log[Z_{\rm im}]$  versus frequency. (e) Plot of  $\log[Z_{\rm in}]$  at 0.5 Hz versus time for 16 exposures of the sensor to solutions having pH values ranging from 2.0 to 9.0. Between exposures, the sensor was equilibrated with pH = 1.0 PBS. (f)  $\log[Z_{\rm im}]$  at 0.5 Hz versus pH calibration plot composed of replicate, nonadjacent exposures to each pH. Impedance data were not fit to an equivalent circuit due to the large impedance of the deprotonated PANI.

indicated in each of the three Nyquist plots. For a gold nanowire with dimensions seen in Figure 3a the measured  $R_{\rm wire}$  is 6.8 k $\Omega$ . This  $R_{\rm wire}$  value coincides with the intercept of the semicircle with the  $Z_{\rm re}$  axis at low frequency, as indicated (Figure 3d). The value of  $Z_{\rm im}=(2\pi f\,C)^{-1}$  is small relative to this 6.8 k $\Omega$  observed for this circuit indicating that because the high impedance of the capacitors at low frequencies "disconnects"  $R_{\rm soln}$  from the circuit. At a high frequency of  $\approx 300$  kHz, the capacitors have negligible impedance, and a second intercept with the  $Z_{\rm re}$  axis is observed (Figure 3d), corresponding to the parallel combination of  $R_{\rm soln}$  and  $R_{\rm wire}$ :  $R_{\rm parallel}=(R_{\rm wire}^{-1}+R_{\rm soln}^{-1})^{-1}$ . Altering the salt concentration and extracting  $R_{\rm soln}$  and  $R_{\rm wire}$  from impedance data (Figure S4) validate the equivalent circuit, showing  $R_{\rm soln}$  decreases with increased salt concentration, while  $R_{\rm wire}$  remains unchanged.

Eliminating the  $R_{\rm wire}$  resistor by forming a nanogap produces the characteristic vertical trace of a series RC circuit (Figure 3e). The intercept of this line with the  $Z_{\rm re}$  axis corresponds to  $R_{\rm soln}$ . We use a constant phase element  $(Q)^{31}$  in place of a capacitor to account for the slope of this trace likely due to the nanoscale heterogeneity in the surface of the nanowire, which results in nonuniform capacitance:  $^{32}$ 

$$Z_{Q} = \frac{1}{Q_{0}(j2\pi f)^{n}} \tag{1}$$

where n is the constant phase  $(-90^{\circ} \times n)$ , with 0 < n < 1. The value of n in the Nyquist plot of Figure 3e is 0.91.  $Q_0$  is the capacitance corresponding to  $n = 1.0.^{31}$  This equivalent circuit was validated (Figure S5) by tracking impedance changes  $R_{\rm soln}$  and  $Q_{\rm dl,wire}$  with salt concentration.

A semicircular Nyquist plot is recovered again when the nanowire with a nanogap is coated with conductive PANI forming a PANI nanojunction and restoring  $R_{\text{wire}}$  (now called  $R_{PANI}$ ). The Nyquist plot for the nanojunction pH sensor shown in Figure 3f was acquired in pH = 3.0 buffer. At this pH, the PANI layer is highly conductive, and the plot resembles that of the solid gold nanowire (Figure 3d) except that  $R_{\text{soln}}$ (6.9 k $\Omega$ ) and  $R_{PANI}$  (80.3 k $\Omega$ ) are higher, where  $R_{PANI}$  should be compared to  $R_{\text{wire}}$ . This is a clear indication that, relative to a solid gold nanowire, the low-frequency impedance of the PANI nanojunction is an order of magnitude higher and dominates the through-wire impedance measured at low frequency. Thus, changes in  $R_{PANI}$  can be assumed to be responsive to the local pH at the PANI nanojunction. Finally, the measured C increases by roughly 2 orders of magnitude, likely because of the pseudocapacitance of the PANI, an electroactive polymer. This equivalent circuit highlights the benefit of using impedance as opposed to measuring a dc resistance, as the resistance of the nanojunction at low frequency is decoupled from the resistance of the solution at high frequency. The difference in the measured  $R_{\text{soln}}$  values

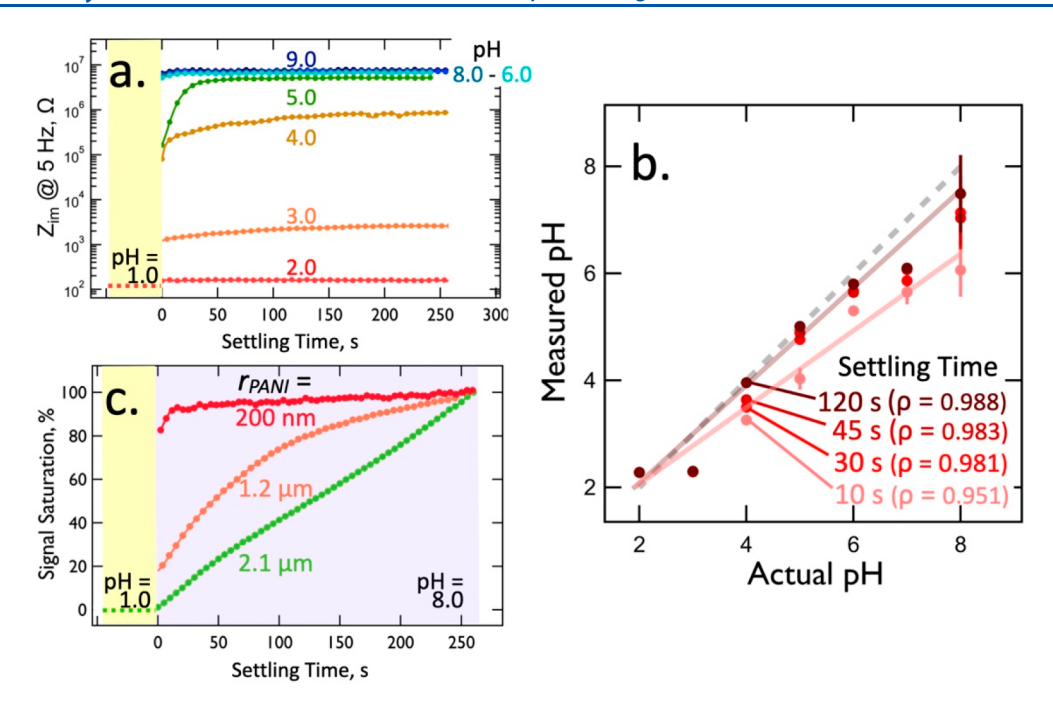


Figure 5. Temporal properties of pH detection. (a)  $\log[Z_{\rm im}]$  at 5 Hz versus time real-time sensing of the PANI nanojunction sensor equilibrated in pH = 1.0 phosphate buffer and exposed to solutions of pH = 2.0 - 9.0 (b) Measured pH versus actual pH for four settling times, as indicated. Covariance of the measured pH from the actual pH was assessed by the Pearson correlation coefficient,  $\rho$ . (c) % signal saturation versus time for three NJ-pH of varying wire radii, encompassing the gold nanowire and the PANI coating. Equilibration of the impedance for the smallest,  $r_{\rm PANI} \approx 200$  nm, occurs within 10 s.

between the three types of nanowires and circuits is likely due to the imperfect surface capacitance at each step in the process. The semicircular Nyquist plot in Figure 3f representing the PANI NJ is much more depressed and nonideal at high frequency compared to the solid gold nanowire Nyquist plot in Figure 3d. This ultimately diminishes the ability to extract an accurate  $R_{\rm soln}$  from the best fit equivalent circuit. However, as will be discussed in a future section, only the impedance at one high frequency is needed to predict  $R_{\rm soln}$  and thus the salt concentration.

Randomized pH Sensing: Properties and Performance of the NJ-pH Sensor. Nyquist plots for pH values from 1.0 to 9.0 (Figure 4a,b) show that at low pH values (<4.0), semicircular Nyquist plots resembling that presented in Figure 3f are observed because the PANI (p $K_a \approx 4$ ) within the nanojunction is conductive in its protonated state. However, the diameter of the semicircle increases sharply as pH increases over this range, from 100 k $\Omega$  (pH = 1.0) to 1.3 M $\Omega$  (pH = 4.0) (Figure 4b). This indicates an increase in resistance of R<sub>PANI</sub> in Figure 4f, as expected. At still higher pH values of ≥5.0, the semicircle disappears, signaling the loss of throughnanojunction conduction. In this pH range, Nyquist plots resemble that of the "open" nanogap as seen in Figure 3e. Low frequency impedance values gradually increase over this pH range (Figure 4a) as protonated PANI is neutralized. Circuit values have been extracted from these Nyquist plots (Figure S6, Table S2).

The dynamic range of the pH response for the NJ-pH sensor can been seen in Bode plots of  $\log Z_{\rm im}$  and  $\log Z_{\rm re}$  versus  $\log f$  (Figure 4c,d). These plots show that the sensitivity of the NJ-pH sensor is greatest at low frequency and is much larger for the  $Z_{\rm im}$  channel than the  $Z_{\rm re}$  channel. At f=0.8 Hz,  $Z_{\rm im}$  increases by 4 orders of magnitude as pH increases from 2.0 to 9.0 (Figure 4d).  $Z_{\rm re}$  by contrast, increases by just  $50 \times$  across

this same pH range. Equations for the imaginary  $(Z_{\text{im,NJ}})$  and real  $(Z_{\text{re,NJ}})$  components of the NJ-pH sensor impedance, eqs 2 and 3, respectively, predict that  $Z_{\text{im,NJ}}$  is more weakly affected than  $Z_{\text{re,NJ}}$ , by  $R_{\text{soln}}$  relative to  $R_{\text{PANI}}$ .

$$Z_{\text{im, NJ}} = \frac{-R_{\text{PANI}}^2 C_{\text{dl}} 2\pi f}{1 + C_{\text{dl}}^2 2\pi f^2 (R_{\text{soln}} + R_{\text{PANI}})^2}$$
(2)

$$Z_{\text{re, NJ}} = \frac{R_{\text{PANI}} + C_{\text{dl}}^{2} R_{\text{PANI}} R_{\text{soln}} (R_{\text{soln}} + R_{\text{PANI}}) 2\pi f^{2}}{1 + C_{\text{dl}}^{2} 2\pi f^{2} (R_{\text{soln}} + R_{\text{PANI}})^{2}}$$
(3)

Real-time, randomized exposures of the NJ-pH sensor to solutions ranging from pH = 2.0 to pH = 9.0 (Figure 4e) show that the PANI nanojunction equilibrates rapidly and completely produces nearly flat peak plateaus approximating ideal sensor response characteristics. In this experiment, the NJ-pH sensor was immersed in a pH = 1.0 solution between each exposure to buffers at higher pH (purple bars). So called "memory effects", in which the amplitude of a sensor response is dependent upon the pH value of the previous exposure, are minimal. Two exposures to the same pH, separated by several exposures to different solutions, produced nearly identical  $Z_{\rm im}$  responses.

The measured value of  $Z_{\rm im}$  at low frequency is strongly correlated with pH (Figure 4f) creating a sigmoidal response function of log  $Z_{\rm im}$  versus pH. While this plot suggests a loss of pH sensitivity at high pH values, >5.0, in fact,  $Z_{\rm im}$  increases substantially, by 4.8 M $\Omega$ , in the pH range 5.0–9.0 enabling measurement of the pH in this range with good signal-to-noise. The pH = 1.0 baseline is stable across 17 separate exposures throughout nearly 5 h.

The plot of  $\log Z_{\rm im}$  versus time (Figure 5a) shows the equilibration of a NJ-pH sensor upon exposure to buffers ranging from pH 2.0 to pH 9.0. More rapid equilibration is

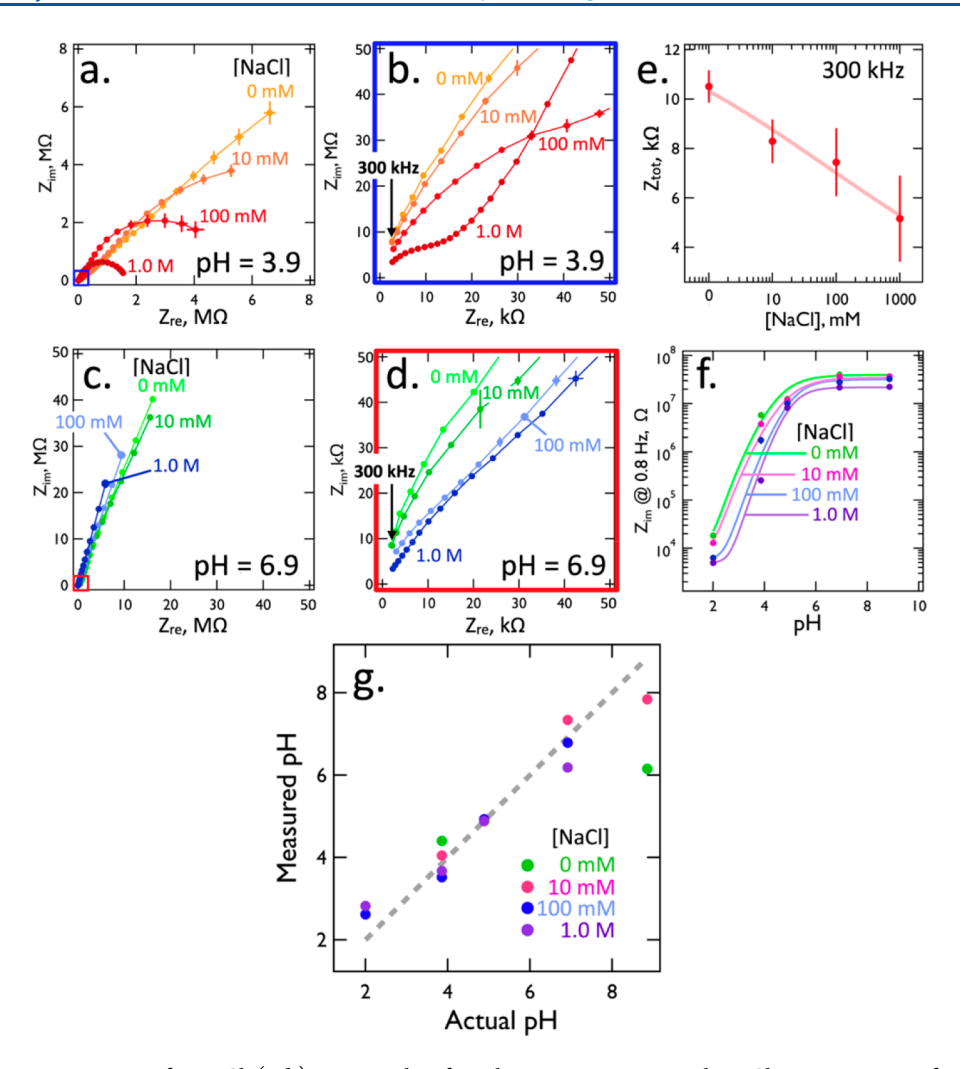


Figure 6. pH measurement correction for NaCl. (a, b) Nyquist plots for solutions at pH = 3.9 with NaCl concentrations of 0, 10, 100 mM and 1.0 M (+50 mM phosphate buffer) as indicated. (c, d) Nyquist plots for solutions at pH = 6.9 with salt concentrations of 0, 10, 100 mM and 1.0 M as indicated. (e)  $Z_{\text{tot}}$  measured at 300 kHz versus NaCl concentration for all data shown in (f). (f) Four  $Z_{\text{im}}$  (measured at 0.8 Hz) versus pH for salt concentrations of 0, 10, 100 mM and 1.0 M (+50 mM phosphate buffer), added to 50 mM phosphate buffer, as indicated. (g) Salt-corrected measured versus actual pH for salt concentrations of 0, 10, 100, and 1.0 M (+50 mM phosphate buffer). Impedance data were not fit to an equivalent circuit due to the large impedance of the deprotonated PANI.

observed at high pH,  $\geq$ 6.0, with response times of <10 s. Equilibration is slower (30–60 s) for solutions of intermediate pH from 3.0 to 5.0. A plot of the pH measured by a PANI nanojunction versus the actual pH measured by a macroscopic glass-membrane pH electrode (Figure 5b) shows the influence of this equilibration behavior on the accuracy of the pH measurements acquired at four settling times (10, 30, 45, and 120 s). The pH measured by the NJ-pH sensor was determined through use of the best fit function from the saturated signal. The degree of correlation between measured pH and actual pH, measured using the Pearson correlation coefficient, r, increases with settling time (where r=1.000 indicates a perfect correlation). At 120 s, r=0.988 indicating excellent correlation, but a high r=0.981 is obtained at a settling time of 30 s.

In view of the nanoscopic dimensions of this pH sensor, is a  $\approx 30$  s response time reasonable? One response rate-limiting process could be the diffusion of  $H_3O^+$  and  $OH^-$  in the PANI, which is required for equilibration of solution-phase concentrations with the polymer. The Einstein equation,  $^{33}$   $t = x^2/(2D)$ , provides the means for estimating the time, t, required

for the diffusion of a species with a diffusion coefficient, D, to diffuse a distance, x. The diffusion coefficient of small ions in electrodeposited PANI is in the range from  $10^{-12}$  to  $10^{-13}$  cm<sup>2</sup>/s.<sup>34</sup> If a diffusion distance of x = 50 nm is assumed, the Einstein equation yields values of t in the range 12.5 s < t < 125 s. The observed time response of the NJ-pH sensor is in the middle of this range. Thus, the slow diffusion of  $H_3O^+$  and  $OH^-$  in the PANI could reasonably account for the measured time response of these sensors, which becomes dramatically slower as the thickness of the PANI coating increases up to 2  $\mu$ m as shown in Figure 5c.

The response times reported here (ranging from 30 s to 2 min for the smallest NJ-pH sensors) are similar to, or somewhat faster than, the response times reported for nanoscopic PANI-based gas sensors for small molecules (30 s to 9 min) including NH<sub>3</sub>,<sup>35</sup> NO<sub>2</sub>,<sup>35</sup> O<sub>3</sub>,<sup>36</sup> and H<sub>2</sub>S.<sup>35,37</sup> The similarity of response times observed for a variety of PANI-based nanoscopic sensor systems and analytes supports the hypothesis that the slow diffusion of analyte species in PANI is rate-limiting in terms of sensor response.

Influence of Salt Concentration on the Accuracy of the NJ-pH Sensor. At low frequencies, f < 1 Hz, the NJ-pH capacitors (Figure 3f) "pinch off" the coupling of charge from the PANI-coated nanowire into the solution, because the impedance of the interfacial capacitor is proportional to 1/f:

$$Z_{\text{Cdl,wire}} = \frac{1}{2\pi f C_{\text{dl}}} \tag{4}$$

In principle, this minimizes the influence of  $R_{\rm soln}$  on the sensor signal. Experimentally, however, we find that the pH calibration of the NJ-pH is affected by the salt concentration of the solution. This observation suggests that the ionic environment surrounding PANI in the nanojunction directly modifies  $R_{\rm PANI}$  through a Donnan equilibrium. Due to the positive charge of PANI in its protonated state, a Donnan-like potential forms at its interface with the solution, opposing the uptake of protons. The strength of this field depends on the anion concentration in the solution, as the anions compensate this charge and diminish the field strength. Thus, the concentration of salt in the solution will alter the nanojunction's protonation state.

Nyquist plots obtained as a function of the salt concentration at constant pH = 3.9 (Figure 6a,b) and pH = 6.9 (Figure 6c,d) show considerable variations as the salt concentration increases from +0.050 M phosphate buffer to 1.0 M. When these impedance data for the full range of pH values are translated into  $Z_{\rm im}$  versus pH calibration curves (Figure 6f), the influence of salt over this concentration range is seen to be approximately 1 pH unit at pH = 4.0, on the rising portion of the calibration curve, but up to 2 pH units at pH > 5, on the rising plateau of the curve. The accuracy issue posed by the variation of the salt concentration is similar to that encountered with conventional glass pH electrodes, where liquid junction potentials, sodium ions, and activity effects combine to introduce pH errors of similar magnitudes.<sup>39</sup>

However, impedance readout of the PANI nanojunction provides a means for correcting the measured pH for the influence of salt. The key is that  $Z_{\text{tot}}$  at very high frequency, f =300 kHz, is logarithmically correlated with the salt concentration, irrespective of pH (Figure 6e). Therefore, the salt concentration of a test solution can be determined at f =300 kHz, and an appropriate calibration curve can be selected for the pH measurement (Figures 6f and S7). This strategy eliminates the deleterious influence of salt on measurement accuracy within the range from 0.05 to 1.05 M except at pH values of >8.0 where measured pH value remains somewhat too low (Figure 6g). The accuracy of the NJ-pH sensors in synthetic urine was also tested and shown in Figure S8. For a synthetic urine solution with a measured pH of 6.62 by a glass pH-electrode, the NJ-pH sensor measured pH is  $6.72 \pm 0.04$ , further confirming that this sensor can accurately predict pH in complex media.

## CONCLUSIONS

A pH sensing "node" that is <100 nm in all three dimensions is realized using a sensor architecture in which a gold nanowire controllably fractured and the resulting nanogap is filled with pH-responsive PANI. Using a frequency of  $\approx$ 1.0 Hz, the electrical impedance measured across the nanogap is used to read the pH in the PANI nanojunction. A second, high frequency impedance measurement allows for the determination of the salt concentration and correction of the measured

pH, if necessary. The use of impedance instead of a dc resistance measurement permits signal to be extracted at pH values well removed from the  $pK_a$  of PANI and at high pH values where PANI has little conductivity. The properties of the PANI nanojunction for measuring pH are similar to those of macroscopic glass membrane electrodes: a pH measurement range of 2.0–9.0, a reversible response, a response time of 30 s, and reusability. However, the dimensions of the PANI nanojunction are less than 100 nm.

It should be emphasized that the NJ-pH sensor is obtained exclusively by high-throughput wet-chemical processing steps and does not require a clean-room, focused ion-beam milling, electron beam lithography, or other time-intensive and expensive microfabrication processes and facilities. Even the LPNE process required to fabricate single gold nanowires is compliant with the atmosphere of a normal wet chemistry laboratory.

A clear path for the generalization of PANI nanojunction pH sensor to the measurement of metal ions, nucleic acids, and proteins is provided by the fact that the required recognition elements (ss-DNA, antibodies, engineered virus particles, chelating agents) have previously been incorporated into the polymer matrix of PANI and other conductive polymers during the electropolymerization process. We look forward to testing this hypothesis in our subsequent investigations of these devices.

#### ASSOCIATED CONTENT

## **Supporting Information**

The Supporting Information is available free of charge at https://pubs.acs.org/doi/10.1021/acs.analchem.2c02606.

Table S1 listing recent examples of nanoscale pH sensors; Table S2 listing best fit values from the randomized pH exposures; Scheme S1 showing poly-(aniline) (PANI) structure and its conductivity in the protonated (emeraldine salt) and deprotonated (emeraldine base) state; Figure S1 showing fabrication process for single poly(aniline) (PANI) nanojunction sensors; Figure S2 showing pH control experiments for a continuous Au nanowirel Figure S3 showing pH controls for empty nanogap within a single Au nanowire; Figure S4 showing experimental data and best fit models for the Au nanowire while varying the concentration of LiClO<sub>4</sub> exposed to the device; Figure S5 showing experimental data and best fit models for the Au nanogap while varying the concentration of LiClO<sub>4</sub> exposed to the device; Figure S6 showing averaged impedance data of the PANI NJ sensor exposed to various solutions of different pH values overlaid with the best fit overlaid; Figure S7 showing a diagram of how one would use the high frequency impedance to correct for the salt effect; Figure S8 showing calibration curves for two separate NJ-pH sensors and the measurement of the pH of a synthetic urine solution (PDF)

#### AUTHOR INFORMATION

### **Corresponding Author**

Reginald M. Penner — Department of Chemistry, University of California, Irvine, California 92697-2025, United States; orcid.org/0000-0003-2831-3028; Email: rmpenner@uci.edu

#### **Authors**

Nicholas P. Drago — Department of Chemistry, University of California, Irvine, California 92697-2025, United States;
ocid.org/0000-0002-3790-552X

Eric J. Choi — Department of Chemistry, University of California, Irvine, California 92697-2025, United States; orcid.org/0000-0003-3287-1284

Jihoon Shin — School of Chemical Engineering, Sungkyunkwan University, Suwon, Gyeonggi-do 16419, South Korea

Dong-Hwan Kim — School of Chemical Engineering, Sungkyunkwan University, Suwon, Gyeonggi-do 16419, South Korea; Occid.org/0000-0002-2753-0955

Complete contact information is available at: https://pubs.acs.org/10.1021/acs.analchem.2c02606

#### Notes

The authors declare no competing financial interest.

#### ACKNOWLEDGMENTS

The authors acknowledge the financial support of this work by the National Science Foundation (Grants CBET-2149631 and CHE-2201042). The scientific leadership of Professor Nongjian Tao and his students are gratefully acknowledged. SEM data were acquired at the Irvine Materials Research Institute (IMRI).

## REFERENCES

- (1) Cremer, M. Z. Biol. 1906, 47, 562-608.
- (2) Hirakawa, S.; Yoshimura, H. Jpn. J. Physiol. 1964, 14, 45-55.
- (3) Aref, M.; Ranjbari, E.; García-Guzmán, J. J.; Hu, K.; Lork, A.; Crespo, G. A.; Ewing, A. G.; Cuartero, M. Anal. Chem. **2021**, 93 (47), 15744–15751.
- (4) Cui, Y.; Wei, Q.; Park, H.; Lieber, C. M. Science **2001**, 293 (5533), 1289-1292.
- (5) Fujisaku, T.; Tanabe, R.; Onoda, S.; Kubota, R.; Segawa, T. F.; So, F. T. K.; Ohshima, T.; Hamachi, I.; Shirakawa, M.; Igarashi, R. ACS Nano 2019, 13 (10), 11726–11732.
- (6) Shen, J.; Xiao, Q.; Sun, P.; Feng, J.; Xin, X.; Yu, Y.; Qi, W. ACS Nano 2021, 15 (3), 4947–4955.
- (7) He, J.; Forzani, E. S.; Nagahara, L. A.; Tao, N.; Lindsay, S. J. Phys.: Condens. Matter 2008, 20 (37), 374120.
- (8) Aguilar, A. D.; Forzani, E. S.; Tao, N. J.; Nagahara, L. A.; Amlani, I.; Tsui, R. *IEEE Sensors Journal.* **2008**, *8*, 269–273.
- (9) Forzani, E. S.; Zhang, H.; Nagahara, L. A.; Amlani, I.; Tsui, R.; Tao, N. *Nano Lett.* **2004**, *4* (9), 1785–1788.
- (10) Díaz Aguilar, A.; Forzani, E. S.; Leright, M.; Tsow, F.; Cagan, A.; Iglesias, R. A.; Nagahara, L. A.; Amlani, I.; Tsui, R.; Tao, N. J. *Nano Lett.* **2010**, *10* (2), 380–384.
- (11) Forzani, E. S.; Li, X.; Tao, N. Anal. Chem. 2007, 79 (14), 5217-5224.
- (12) MacDiarmid, A. G.; Manohar, S. K.; Masters, J. G.; Sun, Y.; Weiss, H.; Epstein, A. J. Synth. Met. 1991, 41 (1-2), 621-626.
- (13) Li, D.; Huang, J.; Kaner, R. B. Acc. Chem. Res. 2009, 42 (1), 135–145.
- (14) Huang, J.; Virji, S.; Weiller, B. H.; Kaner, R. B. J. Am. Chem. Soc. **2003**, 125 (2), 314–315.
- (15) Song, E.; Choi, J. W. Microelectron. Eng. 2014, 116, 26–32.
- (16) Bangar, M. A.; Shirale, D. J.; Chen, W.; Myung, N. V.; Mulchandani, A. Anal. Chem. 2009, 81 (6), 2168–2175.
- (17) Hangarter, C. M.; Hernandez, S. C.; He, X.; Chartuprayoon, N.; Choa, Y. H.; Myung, N. V. Analyst 2011, 136 (11), 2350-2358.
- (18) Liu, H.; Kameoka, J.; Czaplewski, D. A.; Craighead, H. G. *Nano Lett.* **2004**, *4* (4), 671.
- (19) Lee, S.-Y.; Lim, H.; Choi, G.-R.; Kim, J.-D.; Suh, E.-K.; Lee, S.-K. J. Phys. Chem. C **2010**, 114 (27), 11936–11939.

- (20) Xiang, C.; Kung, S. C.; Taggart, D. K.; Yang, F.; Thompson, M. A.; Güell, A. G.; Yang, Y.; Penner, R. M. ACS Nano 2008, 2 (9), 1939–1949.
- (21) Xiang, C.; Kim, J. Y.; Penner, R. M. Nano Lett. 2009, 9 (5), 2133-2138.
- (22) Zhang, H.; Wang, J.; Wang, Z.; Zhang, F.; Wang, S. Synth. Met. **2009**, 159 (3–4), 277–281.
- (23) Menke, E. J.; Thompson, M. A.; Xiang, C.; Yang, L. C.; Penner, R. M. Nat. Mater. **2006**, 5 (11), 914–919.
- (24) Xing, W.; Hu, J.; Kung, S. C.; Donavan, K. C.; Yan, W.; Wu, R.; Penner, R. M. *Nano Lett.* **2012**, *12* (3), 1729–1735.
- (25) Durkan, C.; Welland, M. E. *Ultramicroscopy* **2000**, 82 (1–4), 125–133.
- (26) Hadeed, F. O.; Durkan, C. Appl. Phys. Lett. 2007, 91 (12), 123120.
- (27) Trouwborst, M. L.; Van Der Molen, S. J.; Van Wees, B. J. J. Appl. Phys. **2006**, 99 (11), 114316.
- (28) Strachan, D. R.; Smith, D. E.; Johnston, D. E.; Park, T. H.; Therien, M. J.; Bonnell, D. A.; Johnson, A. T. *Appl. Phys. Lett.* **2005**, 86 (4), 043109.
- (29) Johnston, D. E.; Strachan, D. R.; Johnson, A. T. C. Nano Lett. **2007**, 7 (9), 2774–2777.
- (30) Esen, G.; Fuhrer, M. S. Appl. Phys. Lett. 2005, 87 (26), 263101.
- (31) Brug, G. J.; van den Eeden, A. L. G.; Sluyters-Rehbach, M.; Sluyters, J. H. *Journal of Electroanalytical Chemistry and Interfacial Electrochemistry* **1984**, 176 (1–2), 275–295.
- (32) Alexander, C. L.; Tribollet, B.; Orazem, M. E. *Electrochim. Acta* **2016**, 188, 566–573.
- (33) Islam, M. A. Phys. Scr. 2004, 70 (2-3), 120-125.
- (34) Kanamura, K.; Kawai, Y.; Yonezawa, S.; Takehara, Z. J. Phys. Chem. 1994, 98 (8), 2174–2179.
- (35) Lim, J. H.; Phiboolsirichit, N.; Mubeen, S.; Deshusses, M. A.; Mulchandani, A.; Myung, N. V. Nanotechnology 2010, 21 (7), 075502.
- (36) Srinives, S.; Sarkar, T.; Hernandez, R.; Mulchandani, A. Polymers (Basel) 2017, 9 (12), 80.
- (37) Shirsat, M. D.; Bangar, M. A.; Deshusses, M. A.; Myung, N. V.; Mulchandani, A. Appl. Phys. Lett. **2009**, 94 (8), 083502.
- (38) Chartier, P.; Mattes, B.; Reiss, H. J. Phys. Chem. 1992, 96 (8), 3556-3560.
- (39) Bates, R. G. Determination of pH, Theory and Practice, 2nd ed.; Wiley, 1973.
- (40) Bhasin, A.; Drago, N. P.; Majumdar, S.; Sanders, E. C.; Weiss, G. A.; Penner, R. M. Acc. Chem. Res. 2020, 53 (10), 2384-2394.
- (41) Kindra, L. R.; Eggers, C. J.; Liu, A. T.; Mendoza, K.; Mendoza, J.; Klein Myers, A. R.; Penner, R. M. Anal. Chem. **2015**, 87 (22), 11492–11500.
- (42) Wustoni, S.; Combe, C.; Ohayon, D.; Akhtar, M. H.; McCulloch, I.; Inal, S. Adv. Funct. Mater. 2019, 29 (44), 1904403.
- (43) Bedioui, F.; Devynck, J.; Bied-Charreton, C. Acc. Chem. Res. 1995, 28 (1), 30–36.
- (44) Park, J.; Sempionatto, J. R.; Kim, J.; Jeong, Y.; Gu, J.; Wang, J.; Park, I. ACS Sensors **2020**, 5 (5), 1363–1373.
- (45) Horng, Y. Y.; Hsu, Y. K.; Ganguly, A.; Chen, C. C.; Chen, L. C.; Chen, K. H. Electrochem. Commun. 2009, 11 (4), 850–853.